Materials Chemistry and Physics 151 (2015) 378–384

Contents lists available at ScienceDirect

Materials Chemistry and Physics

journal homepage: www.elsevier.com/locate/matchemphys

Influence of the spray pyrolysis seeding and growth parameters on the structure and optical properties of ZnO nanorod arrays

Juan Rodríguez [a, *], Guy Feuillet [b], Fabrice Donatini [c, d], Diego Onna [e], Luis Sanchez [a], Roberto Candal [e, f], M. Claudia Marchi [e, g], Sara A. Bilmes [e], Frédéric Chandezon [h, i, j]

[a] Facultad de Ciencias, Universidad Nacional de Ingeniería, P.O. Box 31-139, Lima 31, Peru
[b] CEA Grenoble/LETI, 17 rue des Martyrs, F-38054 Grenoble Cedex 9, France
[c] Univ. Grenoble Alpes, Inst NEEL, F-38000 Grenoble, France
[d] CNRS, Inst NEEL, F-38042 Grenoble, France
[e] DQIAQF-INQUIMAE, FCEyN-Universidad de Buenos Aires, Ciudad Universitaria, Pab. II, 1428 Buenos Aires, Argentina
[f] ECyT, 3iA, Universidad Nacional de San Martín, Martín de Irigoyen N° 3100 (1650), San Martín, Pcia de Buenos Aires, Argentina
[g] CMA, FCEyN-Universidad de Buenos Aires, Ciudad Universitaria, Pab. I, 1428 Buenos Aires, Argentina
[h] University Grenoble Alpes, INAC-SPRAM, F-38000 Grenoble, France
[i] CNRS, INAC-SPRAM, F-38000 Grenoble, France
[j] CEA, INAC-SPRAM, F-38000 Grenoble, France

HIGHLIGHTS

- ZnO pyrolytic seeds tuned by the rate of solvent evaporation.
- ZnO NRs grown from tuned pyrolytic seed's structure shows diameter dependence.
- ZnO NRs show stacking faults due to the presence of zinc blende domains.

ARTICLE INFO

Article history:
Received 26 October 2013
Received in revised form
5 December 2014
Accepted 8 December 2014
Available online 11 December 2014

Keywords:
Nanostructures
Semiconductors
Thin films
Vapour deposition
Chemical synthesis
Optical properties

ABSTRACT

ZnO nanorods (NRs) were grown on fluorine doped tin oxide (FTO) substrates at low temperatures (90 °C) from Zn^{2+} precursors in alkaline media previously seeded with ZnO nanoparticles. These were deposited onto the FTO substrate heated at 350 °C by spray pyrolysis of a Zn acetate solution in a water ethanol mixture. The structure of seeds was tuned by the ethanol to water ratio, Γ, which controls the solvent evaporation rate of drops impinging the substrate. From a detailed characterization using a combination of scanning electron microscopy, X-ray diffraction, UV–visible absorption and cathodoluminescence spectroscopies, the dependence of the morphology and optical properties of the ZnO NRs on the seeding conditions was demonstrated. NRs grown on seeds deposited from solutions with Γ in the 0.03–0.06 range – *i.e.* when the surface excess of ethanol in the water–ethanol mixture has a maximum – show thinner average diameters and stacking faults due to the presence of zinc blende domains embedded into an overall wurtzite NR. They furthermore exhibit blue-shifted near band edge emission peak and a high deep level emission in cathodoluminescence. All these findings support the use of spray pyrolysis as a simple and reproducible way to control the seeds deposition, influencing the growth, the structure and the optical properties of the final ZnO NRs.

© 2014 Published by Elsevier B.V.

1. Introduction

Nanostructures made of wide bandgap semiconductors have recently attracted considerable research interest because of their promising applications in optoelectronics, *e.g.* for UV lasers or photovoltaic devices [1–4]. Zinc oxide (ZnO) is one of such semiconductors with a direct bandgap energy E_g around 3.4 eV at room

* Corresponding author.
E-mail addresses: jrodriguez@uni.edu.pe, rodriguezback@gmail.com (J. Rodríguez).

http://dx.doi.org/10.1016/j.matchemphys.2014.12.013
0254-0584/© 2014 Published by Elsevier B.V.

temperature [5]. Other important parameters of ZnO are its negligible toxicity as well as its relatively high exciton binding energy ($E_b = 60$ meV) and its exciton Bohr radius, around 20 Å [6,7], which makes it interesting for room temperature optical applications such as near UV or blue lasing [8–10]. Different growth techniques [1–3,7] have been employed to obtain good quality ZnO nanorods but they usually require high growth temperatures. An alternative simple and cost-effective way to synthesize ZnO NRs films is through wet chemical pathways. This usually involve two steps: the formation of a layer of seeds followed by the growth of the NRs from a Zn^{2+} solution [11,12]. The seeding step can be achieved by several techniques [25]. However spray pyrolysis (SP) has proven to be a successful and low cost procedure for building a layer of seed nanoparticles onto conductive substrates [11–14]. In addition to doping [15–17]; several strategies have also been implemented to vary the optical properties of the NRs: quantum confinement for diameters below 10 nm [7]; varying the growth conditions [18], such as environment [19], temperature [20] and concentration of the zinc source [21], as well as the pH of the growth aqueous solution [22]. Some attempts have also been done to study the effect of seeds on the NRs structure and alignment [23–25]. Recently it was reported that deep level luminescence originates from surface states [26] whose density increase as the NR diameter decreases. However to date and to the best of our knowledge, there has been no study to date showing how the seeds control impacts the optical properties in ZnO NRs.

In this work, we report the growth of ZnO NRs arrays at low temperature (90 °C) from seeds deposited via SP onto Fluorine doped Tin Oxide glasses (FTO). The structure and texture of seeds was tuned by varying the molar ratio of the ethanol to water mixtures, Γ, containing the Zn precursors which is sprayed onto a heated FTO substrate. This seeding step at constant growth in slow kinetics conditions influences the diameter and the density of the NRs, which in turn affects the optical properties of the obtained ZnO NRs films. From a detailed analysis of morphological and crystallographic properties, it was possible to correlate and understand the influence of seeding on the NRs' structure (diameter), crystallinity as well as on their UV–vis absorption and cathodoluminescence (CL) spectra.

2. Experimental section

2.1. Materials

Chemical reactants used as precursors for ZnO seeds and rods were, respectively, analytical grade zinc acetate [$Zn(CH_3COO)_2 \cdot 6H_2O$] and zinc nitrate [$Zn(NO_3)_2 \cdot 6H_2O$] pro analysis (PA) 100% from Fermont. Sodium hydroxide (NaOH) 98% PA, from EKA Chemicals was used for the synthesis of the ZnO seeds and the nanorods growth solution.

FTO conductive glass (Libbey Owens Ford glass substrates coated with a layer of transparent and conducting SnO_2:F having a resistance of 8 Ω/cm^2) was used as the substrate for the growth of ZnO nanorods. FTO-coated glass is well adapted for further electrochemical or photoelectrochemical applications. In practice, 2.0 × 1.5 cm^2 pieces of FTO conductive glass were cleaned in an ultrasonic bath, first with water and then with ethanol, before depositing the seed layer.

2.2. Seed deposition

Zinc oxide seed films were first deposited onto the pre-cleaned FTO-coated glass substrate using spray pyrolysis (SP) technique and were then subsequently used as the substrate to grow ZnO nanorods [13,14].

In a homemade SP technique described in detail elsewhere [14], a medical nebulizer was used as atomizer to produce uniform size droplets which were directed by a nozzle towards the hot substrate (350 °C). The nozzle performed an oscillating movement at constant velocity to scan the whole area of the substrate. The average distance between the nozzle distance and the substrate is 5 mm. The precursor used in all experiments for the present work was a 0.10 M zinc acetate solution (Riedel-de-Haen, Seelze, Germany) in a mixture of deionized water and ethanol. The molar ethanol/water molar ratio (Γ) was varied within the range 0–0.92. Some drops of acetic acid were added to ensure both the total dissolution of zinc acetate and to adjust the pH of the precursor solution to 5.8. Microfiltered air was used as a carrier gas at a fixed pressure of 1.7 × 10^5 Pa with a gas flow maintained at 15 L/min. Compared to previous works where thick films of ZnO were grown (typically several hundreds of nm obtained for 60 min of deposition time) [13,14], in the present case, thin layers (typically less than 100 nm) of ZnO were used as seeds for the growth of the NRs. Typically, this represented about 10 sweeps of our SP setup for the deposition of the seeds corresponding to approx. 30 sec of deposition time [27]. Scanning electron microscope (SEM) images of a typical bare FTO substrate and of seeded substrates with Γ = 0, 0.06 and 0.92 are presented in Fig. S1 (see supplementary material).

2.3. Growth of ZnO NRs films

The solution medium used for the growth of the ZnO NRs was prepared as follows: equal volumes of $Zn(NO_3)_2$ (0.15 M) and NaOH (2.1 M) were mixed under continuous stirring. A white precipitate was formed approximately one minute after mixing. The complete system was aged overnight at 23 °C and filtered under vacuum to obtain a clear solution. In the following, this reference solution will be referred to as having a concentration C_0.

The substrates seeded with ZnO films were placed in a 100 mL screw-capped glass flask (Normax) and the solution medium for the growth of ZnO NRs was added. The concentration of the growth solution was varied between C_0, $C_0/2$ and $C_0/4$. This glass flask containing the substrate and the solution was placed in an oven at 90 °C during 1 h. These parameters were selected in order that ZnO NRs growth occurred in the regime of slow kinetics [8]. The morphology and the structure of the NRs depend on the characteristics of the ZnO seeds as will be discussed below. The substrates covered with ZnO NRs were then removed from the solution, cleaned with water, ethanol and finally dried at 60 °C.

2.4. Characterization methods

The morphology of films and NRs was studied using scanning electron microscopy (SEM) with an ULTRA-55 field emission SEM (Carl Zeiss SMT AG) working at an electron beam energy of 15 keV. Alternatively, a Supra 40 field emission SEM was also used (electron beam energy of 3 keV). Analysis of the rod size distribution was made with the ImageJ software [28]. The crystalline structure of the NRs was determined by X-Ray Diffraction analysis (XRD, Siemens D5000 with Cu-K_α radiation and a graphite monochromator). Transmittances of the films were measured with a UV–vis spectrophotometer (Agilent 8453).

Cathodoluminescence was carried out in a FEI Quanta SEM equipped with a liquid He cryogenic stage in order to cool down the sample from room temperature to 5 K. The luminescence of the sample under electron irradiation was collected through a parabolic mirror into the entrance slit of a Jobin-Yvon HR spectrometer. For CL spectra a nitrogen cooled Si CCD is used, whereas a single channel detector is used for CL mapping. For these experiments, NRs from as-grown samples were mechanically dispersed on to p+

silicon wafers. This allows to study the cathodoluminescence (CL) of isolated NRs lying on a conducting substrate and to avoid charging effects. CL excitation conditions were similar for all samples, namely 30 keV electron beam energy, a beam size of 0.2 μm and a beam current of 1.5 nA. For each sample, a cathodoluminescence image and a CL spectrum were collected together with a SEM image.

3. Results

3.1. Influence of the ethanol to water molar ratio of the seed precursor solution on the diameters of the NRs

Fig. 1 shows SEM images of ZnO NRs grown over seeds deposited by SP formed for three representative ethanol/water ratios: $\Gamma = 0$ (a), $\Gamma = 0.06$ (b). and $\Gamma = 0.92$ (c) NRs exhibit a hexagonal cross-section with average diameter and diameter distribution dependent on the ethanol/water ratio of the solution employed for seeding, as shown in the insets of Fig. 1. Fig. 2 compiles the diameter values with their standard deviation as a function of Γ. These values are also given in Table 1. Both the average diameter and their dispersion exhibit a trend to a minimum for Γ in the range 0.02–0.06. This trend is closely related to the morphology of seeds deposited on the FTO substrate (see Fig. S1 in SI).

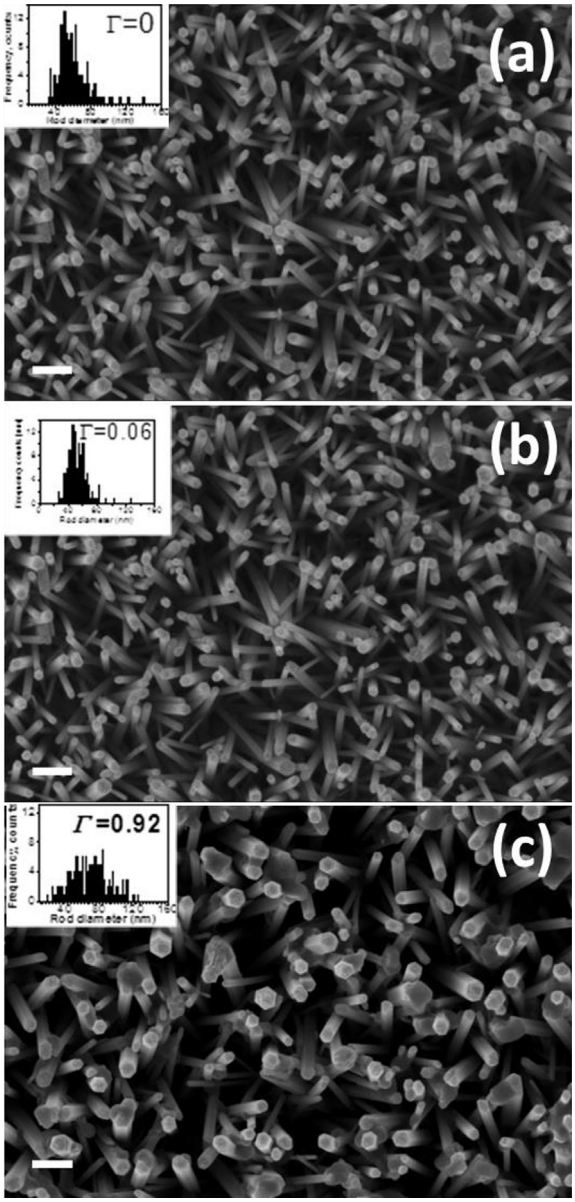

Fig. 1. SEM images of ZnO nanorods grown on FTO substrates with ZnO seeds obtained for an ethanol to water molar ratio Γ of 0 (a), 0.06 (b) and 0.92 (c). The insets in each image represent the histogram of the distribution of diameters for the obtained ZnO NRs as measured from the SEM images. The scale bar corresponds to 200 nm.

3.2. Influence of the concentration of the NRs growth solution on their morphology

To grow the ZnO NRs the seeded FTO substrate was immersed during 1 h in a solution with a concentration of precursors C_o, $C_o/2$ and $C_o/4$ (see 2.3). SEM images obtained for each one of these conditions are displayed in Fig. 3a–f and Fig. 3g–i for $\Gamma = 0$, $\Gamma = 0.06$ and $\Gamma = 0.92$, respectively. The insets in Fig. 3a–c show SEM images at higher magnification and display a clear hexagonal faceting of the ZnO NRs as well as a longitudinal nanostructuration. The main difference between the samples is the average diameter of the nanorods. As can be seen from the SEM images, using a bath of the reference concentration C_o yields ZnO NRs with significantly larger diameters with lower width dispersion and better arrangement than at the less concentrated solutions, namely $C_o/2$ and $C_o/4$.

3.3. Crystallinity and orientation

Fig. 4 shows the results of the XRD θ–2θ analysis of the ZnO NR films grown on seeds deposited by SP. The major peaks in the diffractograms can be ascribed to the hexagonal wurtzite structure of ZnO, corresponding to (002), (101), (102) and (103) planes, with the (002) peak dominating, which indicates that the *c*-axis of the wurtzite structure is the preferential direction of growth of the NRs, as usually observed for ZnO NRs [7,29]. This is markedly different from the diffraction patterns obtained for the seed layers [14]. The crystallite size along the *c*-axis can be estimated for each sample from the Full-Width-at-Half-Maximum (FWHM) of the (002) line using Debye–Scherrer's equation, *i.e.* $D = 0.9\lambda/\beta \cos\theta$ where $\lambda = 1.540598$ Å is the wavelength of the CuKα radiation, θ the diffraction angle and β is the FWHM of the (002) diffraction peak. The calculated crystalline domain size is about 10–15 nm, regardless of the value of Γ.

In addition to the wurtzite peaks, much weaker peaks can be observed in the diffractograms at 2θ values of *ca.* 36°, 42° and 61° (note the log scale in Fig. 4). They correspond to the (111), (200) and (220) diffractions of the zinc-blende cubic crystal structure of ZnO (zb-ZnO) [30]. This indicates the presence of I_1 intrinsic stacking faults in the nanorods in the basal plane leading to the formation of zb-ZnO domains embedded in the predominantly wz-ZnO NRs [31]. This is consistent with the small crystallite size along the long axis

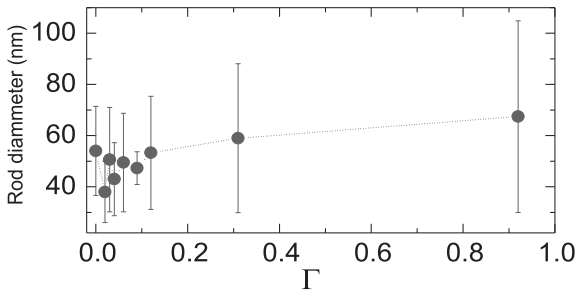

Fig. 2. Influence of the ethanol–water molar ratio Γ used to form the seeds on the average ZnO nanorod diameter.

Table 1
Summary of the results of analysis of the absorption spectra for ZnO NRs samples grown using different ethanol–water molar ratios Γ for the initial seeding conditions (see Fig. 7) and for a bare FTO substrate: thickness of the samples and average diameter of the ZnO NRs as obtained from SEM cross sectional analysis; transmittance at a wavelength of 550 nm; onset of absorption edge as extracted from the extrapolation of the linear part of the absorption spectra (see also S2 in supplementary material for further details).

Sample	Sample thickness (nm)	Average diameter of the NRs from SEM graphs (nm)	Transmittance at 500 nm (%)	Onset of absorption edge (eV)
Bare FTO	346 ± 5		84.3	
Γ = 0	1600 ± 40	54 ± 17	17.3	3.1 ± 0.05
Γ = 0.03	1750 ± 50	51 ± 20	14.1	3.15 ± 0.05
Γ = 0.04	1620 ± 50	43 ± 14	33.6	3.20 ± 0.05
Γ = 0.06	1730 ± 80	49 ± 19	22.5	3.20 ± 0.05
Γ = 0.31	1050 ± 25	59 ± 29	11.3	2.8 ± 0.05
Γ = 0.92	1530 ± 50	67 ± 37	9.2	2.9 ± 0.05

of the NRs determined from the FWHM of the (002) wz-ZnO peak. The low zb-ZnO to wz-ZnO intensity ratio indicates that zb-ZnO represent only a small volume fraction of the NRs. Another point which can be noticed from the data in Fig. 4 is that this ratio is highest for low values of Γ, which denotes that the seeding step plays a major role in the concentration of stacking faults.

3.4. Absorbance in the UV–Vis–NIR

Specular transmittance spectra (T_s) for ZnO NRs arrays were recorded in the $300 < \lambda < 1000$ nm spectral range. In general, the transmittance is below 68% for wavelengths in the NIR (see Table 1, Figs. 5 and S2). The results of this analysis for the different samples grown at C_0 for different seeding conditions Γ are summarized in Table 1. The onset of the absorption edge (see Table 1, the supplementary material for details and refs. [5,32]) presents a noticeable change as a function of Γ with a maximum obtained for Γ = 0.03–0.06 which correlates with the NRs samples having a thinner diameter (Fig. 2) and the highest concentration of zb-ZnO stacking faults (Fig. 4).

Intrinsic values for the bandgap E_g of ZnO at room temperature are around 3.4 eV [5,7], *i.e.* higher than the values for the onset of the absorption edge reported. This fact is probably due that calculated absorption spectra could be influenced by waveguide properties of the ZnO NRs [5]. In addition, reported films present an absorption tail, so called Urbach tail [33], extending towards longer wavelengths, which is mainly ascribed to structural disorder [5,34]. Urbach tail is a common feature in solution grown materials [5,35].

3.5. Cathodoluminescence

Fig. 6 shows the CL spectra measured at RT for samples seeded from solutions with Γ = 0, 0.06 and 0.92 together with corresponding SEM and cathodoluminescence images. Spectra obtained in liquid helium for the same samples are shown in Fig. 7. For each sample, several CL spectra were collected in different areas of the sample and representative ones are presented in Figs. 6 and 7. The CL spectra show two major peaks: one at wavelengths around 370 nm and a much broader one above 450 nm. We attribute the peak at shorter wavelengths to near band edge (NBE) emission of the ZnO NRs, whereas the other one corresponds to deep level (DL) emission [7,37]. Since the visible DL emission band is characteristic of extended defects, a figure of merit for the luminescence of the sample is often taken as the ratio between the intensities of the DL and NBE peaks. The RT and LHe values are reported in Table 2 together with the FWHM of the NBE peaks for samples with seeding conditions Γ = 0, 0.06, 0.92 and concentrations of the growth solution C_0 and $C_0/4$. The NBE emission line at LHe has its maximum at around 3.36 eV for Γ = 0 and 0.92, whereas it is blue-shifted to *ca.* 3.50 eV for the sample with Γ = 0.06. In the latter case, this blue shift goes along with a significant broadening of the NBE line: at LHe temperature, the FWHM for Γ = 0.06 is more than twice broader than for samples with Γ = 0 and 0.92. In addition, the relative height of the deep level emission increases dramatically for Γ = 0.06, where it becomes predominant compared to the NBE line. Taken together, the CL images of the rods for Γ = 0.06 point to strong inhomogeneities in the emission of the NRs. A value of 3.36 eV for the NBE peak position is in the range of the reported

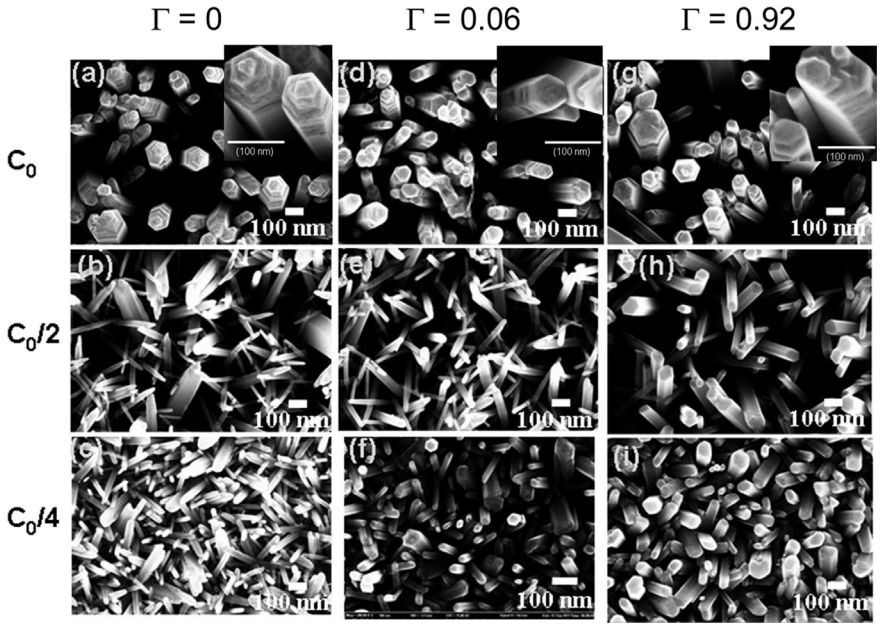

Fig. 3. SEM images of ZnO nanorods grown for various combinations of the ethanol to water ratio molar Γ (seeding conditions) and concentration of the growth solution.

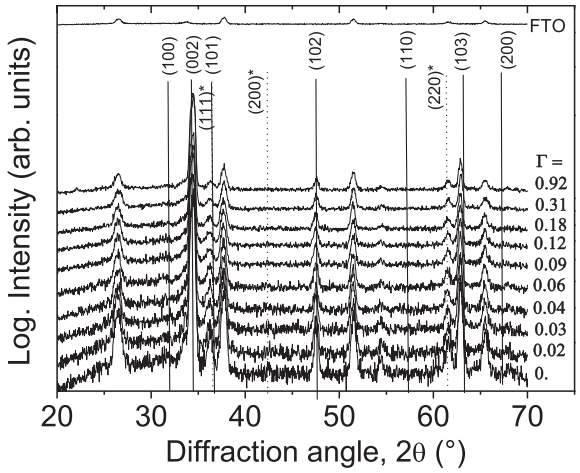

Fig. 4. X-ray diffractograms in logarithmic scale for ZnO nanorods grown on seeds formed with different ethanol–water molar ratio Γ. The diffractogram of the bare FTO substrate is shown as a reference. The three peaks marked with asterisks correspond to positions associated to zinc-blende like ZnO. Other peaks are indexed for wurtzite-like ZnO structure.

values for the gap of bulk ZnO [5,35] but a blue-shifted value of 3.50 eV may arise from other physical effects as discussed below.

4. Discussion

ZnO NRs prepared at low temperature (90 °C) by a wet chemistry route on FTO conductive glasses previously seeded with ZnO nanoparticles by spray pyrolysis exhibit a structure, morphology and optical properties dependent on the ethanol/water ratio of the seeding solution. This dependence is related to the evaporation rate of the solvent when precursors are sprayed on the substrate, thus controlling the growth, morphology and size of the seeds. According to X-ray diffraction analysis, the ZnO NRs possess a predominantly wurtzite crystal structure with their long axis aligned along the *c*-axis and with an average crystallite size around 10–15 nm, as derived from Debye–Scherrer's law. The same XRD data also indicate the presence of zinc blende crystalline domains, and therefore of basal plane stacking faults in the NRs corresponding to the transition between the wurtzite and the cubic phases, the amount of these stacking faults being highly dependent on the synthesis conditions. The formation of such basal plane stacking faults is commonly observed in ZnO NRs and the activation energy to form such defects is as low as *ca.* 15 meV/(unit cell area) [37]. Thus, it is not unexpected that even in a low temperature process as the one used in the present work, such stacking faults can be present.

The blue shift of the absorption onset in the UV–Vis transmittance spectra and of the NBE emission line in the CL spectra may arise from several physical effects. Quantum effects due to transversal confinement are expected to appear for NRs having diameters below 10 nm, while the NRs obtained here have the diameters five times larger [8]. Therefore, in the present case quantum effects cannot be related to transversal quantum confinement. On the other hand, axial quantum confinement due to the zb-ZnO cubic inclusions into the overall wz-ZnO NRs is expected to yield red-shifted emission according to theoretical calculations [36a]. Thus, it cannot account for our observations. Blue shift of the bandgap due to alloying with heteroatoms such as magnesium can also be excluded in our case because of the protocol used to prepare the NRs [5]. A possible explanation for the observed blue shift relies on the fact that in degenerate highly n-doped semiconductors the Fermi level lies above the conduction band minimum, leading to a blue-shift of the absorption edge and of the emission line. This requires that the electron concentration is above the so-called Mott transition, estimated to be around 5×10^{18} cm^{-3} in bulk ZnO [38]. Following this rationale, the doping level of the ZnO NRs, is apparently independent on the growth solution concentration, and dependent on the nucleation layer growth conditions. More specifically, the ethanol to water molar ratio Γ for the seed layer bears a strong influence on the observed NRs blue shifted emission.

The dependence of the ratio between DL and NBE emission in the CL spectra and the observed blue shift of the absorption onset (Fig. 5, Table 1) and of the near band edge emission line in the CL spectra (Figs. 6 and 7, Table 2) call for complementary explanations. Although the origin of deep level emission is still a matter of discussion, it was previously shown that surface-states emission can become predominant when the diameter of the NRs decreases below 100 nm [26]. This is the range of the diameters measured for the NRs in the present work (Figs. 1 and 2) and we therefore may attribute the DL peaks in the CL spectra to a surface state recombination. The DL emission line shows the highest intensity for the NRs corresponding to seeding conditions with $\Gamma = 0.06$. Indeed, the seed layer growth conditions could lead to layers with different extrinsic or intrinsic impurity concentrations, which could out-diffuse towards the nanowires. For the NRs grown at low temperatures (90 °C), only intrinsic point defects (namely Zn_i and O_i) could out-diffuse from the seed layer towards the NRs, since their diffusion activation energies is very low (typically below 0.5 eV) [39].

The singularities observed in NR diameter, zb/wz phase proportion, band edge absorption, DL emission and position of NBE peak in CL spectra when NRs are grown on seeds deposited from precursors dissolved in ethanol–water mixtures with $0.03 \leq \Gamma \leq 0.06$ gives a good evidence that the shape, composition and structure of seeds controls the growth of NRs [25]. The surface excess of ethanol in water presents a maximum for Γ in the 0.03–0.06 range which corresponds to the formation of a monolayer induced by hydrophobic hydration [40]. That means that within this composition range, evaporation of the solvent containing the Zn precursors is faster than water where Zn^{2+} is more soluble. This would produce uncontrolled nucleation and growth processes that lead to seeds formed by aggregated clusters, with higher density of grain boundaries. This is supported by the comparison of the SEM images between the seeded substrates for $\Gamma = 0.06$ and 0.92 which show a striking difference in terms of the size of the seeds (see Fig. S1). This kind of substrate promotes growth from solution mainly controlled by a cluster mechanism instead of an ion-by-ion mechanism. The latter usually promotes more ordered structures and epitaxial-like growth from solution [41] and is likely to occur when growth is conducted on more crystalline seeds as those formed from water ($\Gamma = 0$) or from ethanol rich mixtures ($\Gamma = 0.92$). Moreover, the nanoparticles formed on the FTO substrate from mixtures with Γ in the 0.03–0.06 range exhibit higher dissolution rate (see Ref. [17]), thus the growth of NRs also competes with dissolution of seeds producing a more disordered crystallization over the entire NR. As a consequence of both processes – cluster mechanism and simultaneous dissolution – NRs are thinner and with higher defect density. This explains the optical features in the CL emission spectra and the shift of the near band edge CL emission peak with Γ.

5. Conclusion

In this work we demonstrate that growth of ZnO arrays can be performed by a low cost method of growth from precursors in solution on ZnO seeds deposited by spray pyrolysis on a FTO

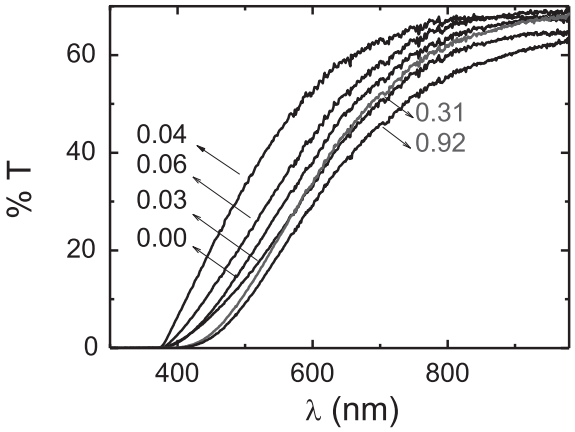

Fig. 5. Transmittance spectra at room temperature for ZnO NRs samples grown using different ethanol–water molar ratios Γ for the initial seeding conditions and a growth solution with concentration C_0.

substrate. Such materials could be suitable for solar active devices such as dye-sensitized solar cells or photocatalytical devices for water decontamination. Although growth conditions influences the properties of the final material, the composition of seeding

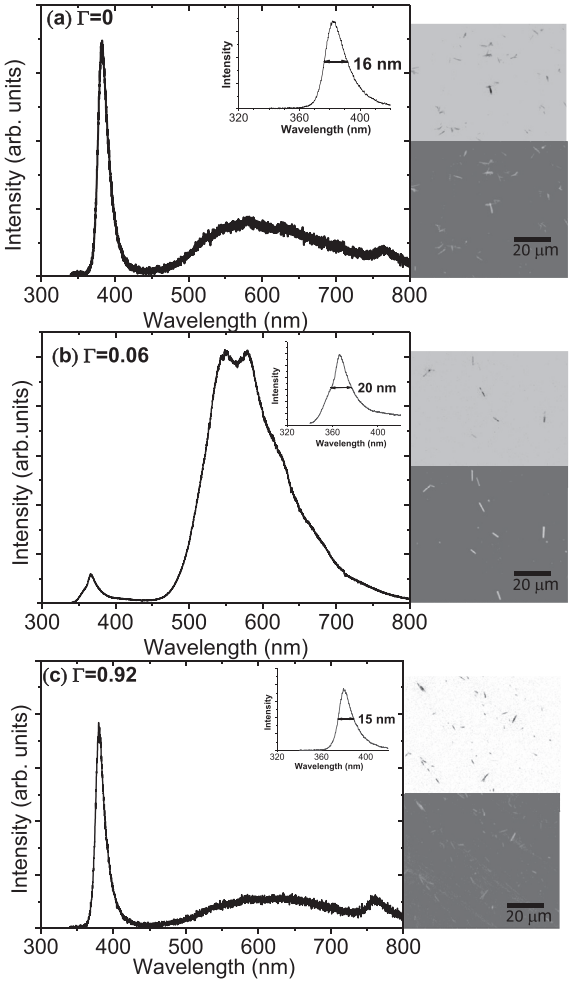

Fig. 6. Room temperature CL spectra of ZnO NRs grown on seeds formed from solutions with the ethanol–water molar ratio: (a) Γ = 0; (b) Γ = 0.06; (c) Γ = 0.92. The inset in each graph shows an enlargement of the near band edge (NBE) peak of the NRs. The images at the right of each graph correspond to the cathodoluminescence (top) and SEM (bottom) images of the sample.

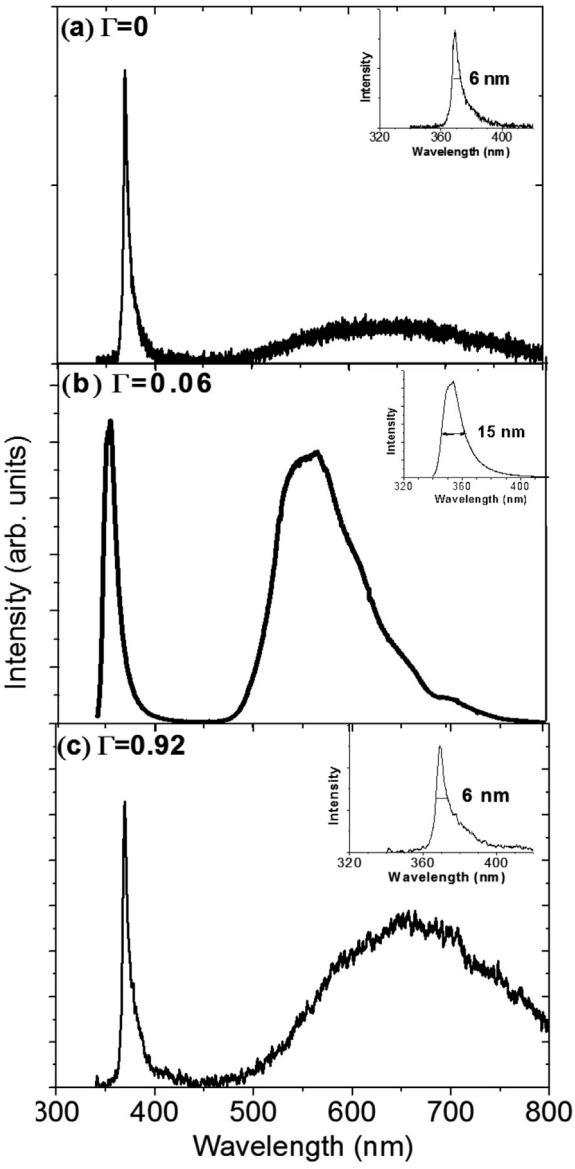

Fig. 7. Liquid helium temperature CL spectra of ZnO NRs grown in the same conditions of Fig. 6.

Table 2
Summary of the cathodoluminescence (CL) analysis at liquid He and at room temperature for samples grown using different ethanol–water molar ratios Γ for the initial seeding conditions and concentrations of the solution medium for the growth of the ZnO NRs. The values of the position of the near band-edge (NBE) peak and its full width at half maximum (FWHM) are given. I_{DL}/I_{NBE} is the ratio of the intensities of the peaks corresponding to deep level emission (for wavelengths larger than 450 nm) and to NBE, respectively. This value is the average of measurements for different NRs. For the sample with Γ = 0.92 and $C_0/4$, the CL intensity was too low to provide reliable values of the bandgap E_g of the FWHM of the NBE peak.

	Γ	0	0	0.06	0.06	0.92	0.92
	Growth solution	C_0	$C_0/4$	C_0	$C_0/4$	C_0	$C_0/4$
LHe	NBE peak position (eV)	3.36 eV	3.37 eV	3.50 eV	3.49 eV	3.36 eV	3.36 eV
	FWHM of the NBE peak (nm)	6	8	15	19	6	9
	I_{DL}/I_{NBE} ratio	1/7	1/45	1/1	1/6	1/2	1/2
RT	NBE peak position (eV)	3.23 eV	3.23 eV	3.36 eV	3.42 eV	3.27 eV	NA
	FWHM of the NBE peak (nm)	16	20	20	31	15	NA
	I_{DL}/I_{NBE} ratio	1/3	1/10	10/1	1/1	1/2	3/1

solution – in particular, the ethanol molar fraction in the solvent – is the relevant parameter for controlling the structure and optical properties. The technique used in this work is a novel low temperature, and thus low cost method that could be extended to other metal oxide nanostructured materials.

Acknowledgements

This work was supported by the Fincyt Project N°140-FINCYT-IB-2013, the Peruvian-Argentinian 321-2009-CONCYTEC OAJ Project and MINCYT-CONCYTEC PE/09/01, UBACyT 20020100100636; CONICET GI-PIP 11220110101020; PICT-2012-1167. MCM, RJC and SAB are members of CONICET. Dimitry Aldakov is gratefully acknowledged for careful reading of the manuscript. One of the authors, J. Rodriguez, acknowledges the Regional French Cooperation for the Andean countries of the French embassy in Lima, the Nanoandes network and the Puya de Raimondi association for partial financial support.

Appendix A. Supplementary data

Supplementary data related to this article can be found at http://dx.doi.org/10.1016/j.matchemphys.2014.12.013.

References

[1] J. Yang, J. Zheng, H. Zhai, X. Yang, L. Yang, Y. Liu, J. Lang, M. Gao, J. Alloys Compd. 489 (2010) 51.
[2] A.B. Djurišić, X. Chen, Y.H. Leung, Ng Man Ching, J. Mater. Chem. 22 (2012) 6526.
[3] Ü. Özgur, D. Hofstetter, H. Morkoc, Proc. IEEE 98 (2010) 1255.
[4] J. Bouclé, J. Ackermann, Polym. Int. 61 (2012) 355.
[5] C. Klingshirn, J. Fallert, H. Zhou, J. Sartor, C. Thiele, F. Maier-Flaig, D. Schneider, H. Kalt, Phys. Status Solidi B 247 (2010) 1424.
[6] R.T. Senger, K.T. Bajaj, Phys. Rev. B 68 (2002) 045313.
[7] G.–C. Yi, C. Wang, W. Il Park, Semicond. Sci. Technol. 20 (2005) S22.
[8] T. Makino, K. Tamura, C.H. Chia, Y. Segawa, M. Kawasaki, A. Ohtomo, H. Koinuma, Phys. Rev. B 65 (2002) 121201.
[9] X.F. Duan, Y. Huang, R. Agarwal, C.M. Lieber, Nature 421 (2003) 241.
[10] C. Sheng, W. Guoping, Z. Weihang, L. Yuqing, C. Leonid, Z. Jianze, K. Jieying, L. Lin, R. Jingjian, L. Jianlin, Nat. Nanotech. 6 (2011) 506.
[11] L. Vayssieres, Adv. Mat. 15 (2003) 464.
[12] Y. Tang, J. Chen, D. Greiner, L. Ae, R. Baier, J. Lehmann, S. Sadewasser, M.C. Lux-Steiner, J. Phys. Chem. C 115 (2011) 5239.
[13] M. Quintana, E. Ricra, J. Rodríguez, W. Estrada, Catal. Today 76 (2002) 141.
[14] M. Quintana, J. Rodríguez, J. Solís, W. Estrada, Photochem. Photobiol. 81 (2005) 783.
[15] L. Yanmei, W. Tao, S. Xia, F. Qingqing, L. Qingrong, S. Xueping, S. Zaoqi, Appl. Surf. Sci. 257 (2011) 6540.
[16] D. Shuang, J.B. Wang, X.L. Zhong, H.L. Yan, Mat. Sci. Semicond. Proc. 10 (2007) 97.
[17] S. Baek, J. Song, S. Lim, Phys. B 399 (2007) 101.
[18] M. Wang, C.-H. Ye, Y. Zhang, G.-M. Hua, H.-X. Wang, M.-G. Kong, L.-D. Zhang, J. Cryst. Growth. 291 (2006) 334.
[19] B. Dierre, X.L. Yuan, T. Sekiguchi, Microelectr. J. 40 (2009) 262.
[20] M. Guo, P. Diao, X. Wang, S. Cai, J. Solid State Chem. 178 (2005) 3120–3215.
[21] S. Hirano, N. Takeuchi, S. Shimada, K. Masuya, K. Ibe, H. Ysunakawa, M. Kuwabara, J. Appl. Phys. 98 (2005), 094305/1-09430.5/7.
[22] U. Pal, P. Santiago, J. Phys. Chem. B 109 (2005) 15317–15321.
[23] Y. Tak, K. Yong, J. Phys. Chem. B 109 (2005) 19263–19269.
[24] J. Song, S. Lim, J. Phys. Chem. C 111 (2007) 596–600.
[25] L.E. Greene, M. Law, H.D. Tan, M. Montano, J. Goldberger, G. Somorjai, P. Yang, Nano Lett. 5 (2005) 1231–1236.
[26] I. Shalish, H. Temkin, V. Narayanamurki, Phys. Rev. B 69 (2004) 245401.
[27] J. Rodríguez, F. Paraguay-Delgado, A. López, J. Alarcón, W. Estrada, Thin Solid Films 519 (2010) 729.
[28] Image J: http://rsbweb.nih.gov/ij/.
[29] International Center for Diffraction Data, 2011. File 00-001-1136.
[30] International Center for Diffraction Data, 2011. File 03-065-0523.
[31] M.-C. Jeong, S.-W. Lee, J.-M. Seo, J.-M. Myoung, Nanotechnology 18 (2007) 305701.
[32] K.-S. Ahn, S. Shet, T. Deutsch, C.-S. Jiang, Y. Yan, M. Al-Jassim, J. Turner, J. Power Sources 176 (2008) 387.
[33] F. Urbach, Phys. Rev. 92 (1953) 1324.
[34] I. Hamberg, C.G. Granqvist, K.-F. Berggren, B.E. Sernelius, L. Engström, Phys. Rev. B 30 (1984) 3240.
[35] S.A. Bilmes, P. Mandelbaum, F. Alvarez, N. Victoria, J. Phys. Chem. B 104 (2000) 9851.
[36] (a) M.A. Reshchikov, H. Morkoç, B. Nemeth, J. Nause, J. Xie, B. Hertog, A. Osinsky, Phys. B 358 (2007) 401–402.
[37] Y. Yan, G.M. Dalpian, M.M. Al-Jassim, S.-H. Wei, Phys. Rev. B 70 (2004) 193206.
[38] A. Schleife, C. Rödl, F. Fuchs, K. Hannewald, F. Bechstedt, Phys. Rev. Lett. 107 (2011) 236405.
[39] A. Janotti, Chris G. Van de Walle, Phys. Rev. B 76 (2007) 165202.
[40] Y.F. Yano, J. Colloid Interface Sci. 284 (2005) 255.
[41] G. Hodes, Phys. Chem. Chem. Phys. 9 (2007) 2181.